Mechanisms of Porosity Formation during Solidification: A Theoretical Analysis

GEOFFREY K. SIGWORTH and CHENGMING WANG

The formation of porosity during solidification is of great commercial importance and scientific interest. This is particularly so for the question of the "feeding length" of a riser. In this work, a number of theoretical models are derived and their predictions are compared to experimental observations. The comparisons show that in directional solidification, a "thermodynamic" model is useful in predicting when porosity may form. The amount of porosity predicted is too high, however, since it ignores the nucleation of the pore and growth by diffusion of dissolved gas to growing pores. A surprising conclusion of this study is that Darcy's law does not appear to be a controlling factor in porosity distribution or formation. In particular, Darcy's law cannot explain feeding length measurements made in steel castings. A simple "geometrical" criterion is presented instead to describe when shrinkage porosity will occur. This new model suggests a number of interesting experiments, which are proposed in discussion.

I. INTRODUCTION

CASTINGS are an important industrial raw material, and the properties of a casting determine, to a large extent, the quality of the final commercial product. In particular, porosity or shrinkage voids are usually undesirable. From our commercial experience, it appears that one half to three quarters of scrap castings are lost because of porosity and shrinkage.

From a scientific point of view, the problem of porosity formation is complex and most interesting. The thermal properties of the alloy being cast (latent heat of fusion and thermal conductivity), the composition of the alloy (freezing range and dissolved gas content), the mold properties, and the geometry of the casting are all important to the properties of the final cast product. However, we do not know the relative effect of these variables, except in the qualitative way which comes from years of producing castings. The problem has been studied in detail for nearly 50 years, but there appears to be no clear agreement as to which mechanisms control the formation of porosity and shrinkage.

In the absence of a clear scientific understanding, foundrymen have used empirical rules to design their molds. Chvorinov's rule is used to calculate the correct size of the riser, and it is well known that the riser can only feed a certain characteristic distance, called the feeding length. These rules were first observed and codified in the pioneering studies of Pellini,[1,2] and they are still valid and useful today.

Since Pellini's observations are of some importance to the theoretical analysis proposed in this study, it is useful to consider them briefly in detail. The feeding length of a riser is best considered by examination of Figure 1, taken from Pellini's original article.[2] The data presented are for a steel bar cast in green sand. The distance from the riser to the end of the casting is sufficiently long that there is a central section which is "semi-infinite." In this region, the solidification proceeds as if the bar had no ends and were infinitely long. In other words, the temperature in this region is uniform along its length, so the entire section freezes at the same time. Consider the experimental freezing velocity curve at the lower right-hand section of the figure. Five minutes after pouring, a shell 1.5-inches (40-mm) thick from the end has formed at the centerline of the bar. At 10 minutes, there is a region 3-inches (80-mm) thick which is completely solid. At 16 minutes, this shell has reached the right-hand end of the semi-infinite region, whose entire section now freezes. The freezing "wave" then slows down as it approaches the hot riser.

Pellini[1,2] observed centerline shrinkage in these central "semi-infinite" sections of plate and bar castings and in regions adjoining the semi-infinite region. An analysis of his cooling curves showed that in 2-inch- (50-mm-) thick plates, shrinkage porosity occurred in areas where the temperature gradient* was less than 1 to 2 F/in. (20 °C to 40 °C/m). In 4-inch (100-mm) bars, a higher gradient* was required to prevent centerline shrinkage: 6 to 12 F/in. (120 °C to 240 °C/m). Pellini made a number of steel plate castings whose length from riser to end varied. He found that the total length of the plate could be as much as 4.5 times the thickness of the plate. Longer plate sections developed centerline shrinkage. In bar castings, the total feeding length was equal to six times the square root of the thickess.

Niyama *et al.*[3] examined a number of commercial castings and proposed that the temperature gradient (as predicted from computer models of the solidifying castings) could be used to predict the formation of shrinkage

*The gradient referred to here is the component of the temperature gradient in the feeding direction. In this article, the feeding direction is always labeled by the x-axis, which runs from the end of the casting to the riser. In Figure 1, the solidification of the casting is predominantly in a direction perdendicular to the feeding direction and normal to the top and bottom sidewalls of the mold. Thus, Figure 1 represents a case of "nondirectional" solidification, where freezing and feeding are not in the same direction. Shrinkage porosity only occurs in nondirectional solidification and is different from the dispersed microporosity found in "directionally" solidified castings, where freezing and feeding occur in the same direction.

GEOFFREY K. SIGWORTH, Principal Engineer, and CHENGMING WANG, Analysis Engineer, are with Concurrent Technologies Corporation, Johnstown, PA 15904.

Manuscript submitted December 13, 1991.

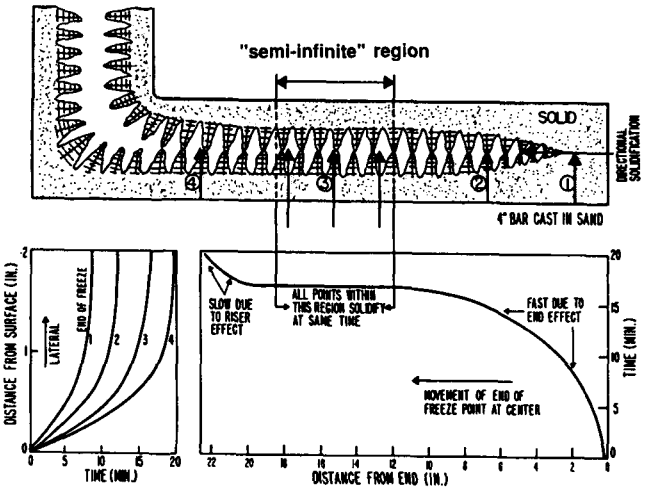

Fig. 1—Solidification of a bar casting whose length is sufficient for the appearance of a semi-infinite region devoid of end effects. (Solidification times are measured by thermocouples.[2])

porosity. Unfortunately, as these researchers clearly recognized, the gradient required to avoid porosity depends on the geometry and size of a particular casting and could not be predicted *a priori*. As their study continued, Niyama *et al.*[4] discovered that both the scale of the porosity and the dendritic structure varied in proportion to the size of the casting. This led them to consider in detail the effect of casting size and resulted in the observation that the critical temperature gradient (required to avoid shrinkage porosity) is related to the time of solidification. Their data for cylindrical steel sand castings are given in Figure 2.

Other researchers have studied the formation of shrinkage porosity by offering theoretical models or empirical prediction criteria (G/R and $G/\sqrt{R}$ and are two common themes), but a review of the literature[5] shows that no consensus has emerged. Consequently, further study appears to be warranted.

When there is directional solidification, no shrinkage

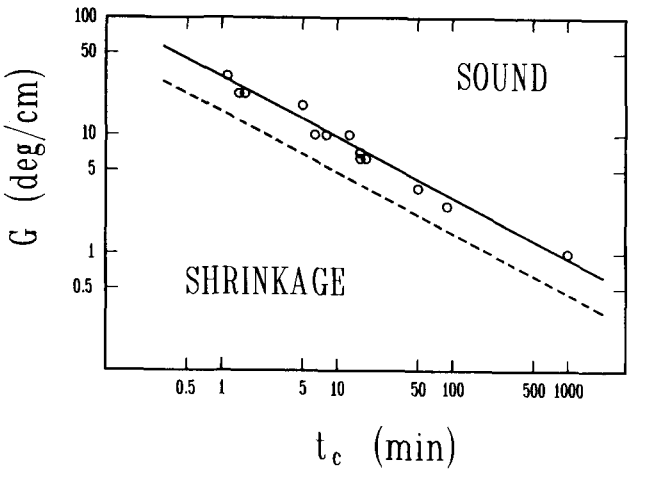

Fig. 2—Relation between the critical temperature gradient and the total solidification time. (The solid curve is the calculated gradient in fully solid region as originally reported. The dashed line is the average gradient in the solid-liquid region.[4])

porosity forms, but undesirable micropososity often occurs. Experimental evidence shows that the size and amount of porosity formed are strongly dependent on the freezing rate and the amount of dissolved gas in the metal. It appears from computer calculations that the "thermodynamic" model offered by Kubo and Pehlke[6] and Poirier and co-workers[7,8] may be used to describe the formation of microporosity. It is worthwhile to examine these models, for simple castings, by integrating the appropriate differential equations exactly instead of numerically. It is also useful to reconsider the "thermodynamic" model in light of the excellent experimental data given to us recently by Fang and co-workers.[9,10]

II. THEORY OF POROSITY FORMATION

A. *Directional Solidification*

In many respects, the situation easiest to consider theoretically is the directional solidification of a casting. Consider the plate shown in Figure 3. The top and bottom walls of the mold are perfect insulators. (This can be produced experimentally by heating these surfaces.) Consequently, solidification proceeds in one direction, parallel to the feeding direction. A detailed schematic view of the solid-liquid region is shown in Figure 4. The total length of the two-phase region is l. This length is

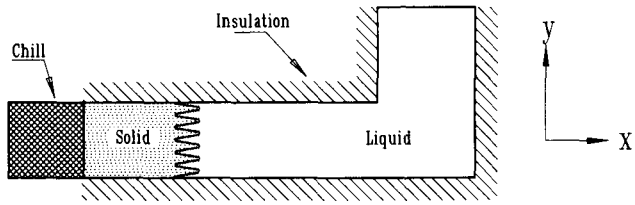

Fig. 3—Schematic illustration of the unidirectional solidification of a plate.

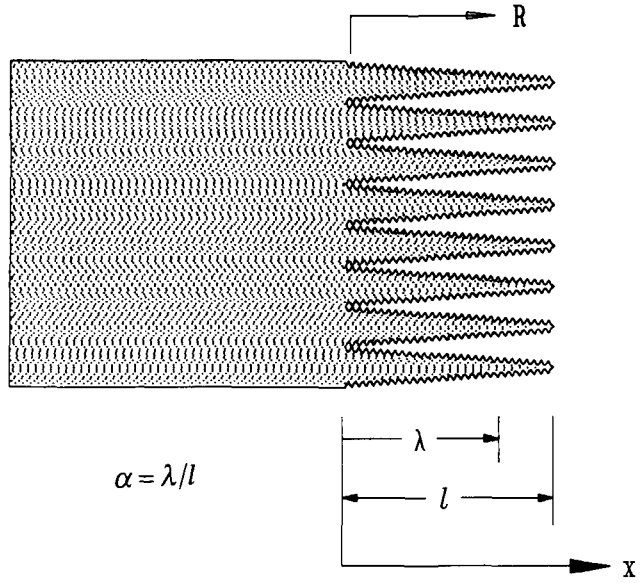

Fig. 4—Detail of the solid-liquid region in Fig. 3.

divided into the portion $\lambda = \alpha l$, where liquid must "filter through" a coherent network of solid dendrites, and a portion where mass feeding may occur (and where little problem with feeding is expected). The experimental evidence available suggests that solid coherency begins to occur at a fraction solidified, f_s^c, equal to about 0.2 or 0.3 in large-grained aluminum alloys.[11-14] Grain refinement increases this to about 0.4 to 0.6. Corresponding values reported for f_s^c in large-grained and refined Cu-10 pct Sn alloys are 0.5 and 0.7.[11]

In the following analysis, the continuity equation is first used to establish the flow of metal needed to feed the solidification shrinkage. Then Darcy's law is applied to calculate the pressure drop required to drive the liquid flow. Mathematical calculations show that this pressure drop is very small and may be ignored without error. Then the "thermodynamic" model is considered. That is, porosity is assumed to form when the "chemical" pressure of dissolved gas (as given by standard segregation equations) balances the sum of the surface tension pressure inside the pore and the local hydrostatic or "mechanical" pressure. The nucleation of the pore and the subsequent growth of the pore by diffusion of dissolved gas are both ignored.

To simplify the mathematical analysis, we assume that the volume fraction of liquid is linear in the two-phase region. That is,

$$g_l = x/l = x(G/\Delta T) \qquad [1]$$

From the conservation of mass, from the fact that the solid is unable to move in the region of coherency, and when no gas porosity is formed, we have

$$\nabla \cdot (\rho_l g_l V_l) + \frac{\partial \rho}{\partial t} = 0 \qquad [2]$$

where

$$\rho = g_l\rho_l + g_s\rho_s = \rho_s(1 - \beta)g_l + g_s\rho_s$$

and

$$\rho_l = \rho_s(1 - \beta) \quad \text{and } \beta = \frac{\rho_s - \rho_l}{\rho_s}$$

Therefore,

$$\frac{\partial \rho}{\partial t} = \rho_s(1 - \beta)\frac{\partial g_l}{\partial t} + \rho_s\frac{\partial g_s}{\partial t} = \rho_s\beta\frac{\partial g_s}{\partial t} \qquad [3]$$

The derivative of fraction solidified with time may be determined from the growth rate as follows:

$$R_x = \frac{\partial x}{\partial t} = l\frac{\partial g_s}{\partial t} \qquad [4]$$

From Eqs. [1] through [3], we obtain

$$\nabla \cdot (g_l V_l) = \frac{-\beta}{1 - \beta}\frac{\partial g_s}{\partial t} = \frac{-\beta}{1 - \beta}\frac{R}{l} \qquad [5]$$

The product $g_l V_l$ is numerically equal to the volumetric flow rate of liquid passing through a planar section of unit area normal to the x-axis. Equation [5] therefore describes the rate of change of the liquid volume flow, caused by solidification shrinkage, as we move through the mushy zone. At the point where $g_s = 1$, this term is zero. Hence, at any distance, x, from the advancing solid interface, we have

$$g_l V_l = \frac{-\beta R}{1 - \beta}\frac{x}{l} = \frac{-\beta R}{1 - \beta}g_l$$

or

$$V_l = \frac{-\beta R}{1 - \beta} \qquad [6]$$

The result is surprising, until the geometry of the situation is considered. Although the total volumetric flow increases as we move in the positive x-direction, the fraction of liquid also increases in proportion, so that the velocity remains constant for this case of directional solidification.

We now consider the application of Darcy's law to the flow of liquid through the semisolid dendritic region:

$$V_x = \frac{-K}{\mu g_l}\frac{\partial P}{\partial x} \qquad [7]$$

where V_x = the linear flow velocity of liquid at any distance, x, from the riser;
K = the specific permeability of the solid dendrites;
μ = the viscosity of the liquid; and
g_l = volume fraction liquid at the point under consideration.

The permeability may be estimated by applying the Hagen-Poiseulle equation:

$$K = \frac{g_l^2}{8n\pi\tau^3} \qquad [8]$$

where n = the number of flow channels per unit area; and
τ = the tortuosity of the flow channels.

Equation [8] is valid when g_l is less than about 0.3,[15,16] which is the region of interest. (The restriction to flow will be the greatest at the end of solidification.) Combining Eqs. [1], [5], [7], and [8] and rearranging, we find that

$$\Delta P = -\frac{\mu}{K}g_l V_l \partial x = \frac{\mu\beta R_x}{(1 - \beta)}8n\pi\tau^3\int_\lambda^x \frac{\partial x}{g_l} \qquad [9]$$

Notice that we are integrating from the point where mass feeding stops to a point somewhere deep inside the two-phase mushy zone. From Eq. [1], we have $\partial g_l = (G/\Delta T)\partial x$; hence,

$$\int_\lambda^x \frac{\partial x}{g_l} = \frac{\Delta T}{G}\int_\alpha^{g_l}\frac{\partial g_l}{g_l} = -\frac{\Delta T}{G}\ln\frac{\alpha}{1 - g_s} \qquad [10]$$

Consequently, the pressure drop with distance is given by

$$\Delta P = \frac{\mu\beta}{(1 - \beta)}8n\pi\tau^3\frac{R_x\Delta T}{G_x}\ln\frac{\alpha}{1 - g_s} \qquad [11]$$

The tortuosity is generally not dependent on the rate

of solidification,[16] but as noted by Lee *et al.*,[17] the number of flow channels is inversely proportional to the square of the primary dendrite arm spacing, which is itself a function of the local solidification time:

$$d_1 = \gamma(t_f)^{1/3}$$

Consequently, Eq. [11] becomes

$$\Delta P = \frac{\mu\beta}{(1-\beta)} \frac{8\pi\tau^3}{\gamma^2} \frac{R_x \Delta T}{G_x (t_f)^{2/3}} \ln \frac{\alpha}{1-g_s} \qquad [11a]$$

The grouping $R/G(t_f)^{2/3}$ was proposed by Lee *et al.*[17] to describe the porosity observed in plate castings of A356 alloy. Note that subscripts are used in Eq. [11] to indicate the directional component of G and R.

At this point, it is useful to consider the validity of the mathematical model. Two assumptions were used to derive Eq. [11]. They are

(1) steady-state flow of liquid is assumed by Darcy's law, and
(2) the fraction solid is a linear function of distance.

If one calculates the force of acceleration on the interdendritic liquid, the first assumption is seen to be valid under normal casting conditions. Regarding the second assumption, we would generally not find the fraction of solid to be a linear function of distance in the mushy zone. However, it is a simple matter to account for any nonlinearity by introducing a dimensionless constant in Eq. [1] for the region of interest ($0 \le x \le \lambda$). That is,

$$g_l = \xi \frac{x}{l}$$

For this case, it follows that Eq. [11] becomes

$$\Delta P = \frac{\mu\beta\xi}{(1-\beta)} 8n\pi\tau^3 \frac{R_x \Delta T}{G_x} \ln \frac{\alpha}{1-g_s} \qquad [11b]$$

We now shall calculate the effect of dissolved gas by considering the thermodynamic arguments proposed by Poirier *et al.*[7] and by developing a modified model for this case. The results will then be compared to the data provided by Fang and Granger.[9]

When there is complete diffusion of hydrogen in the solid, the liquid composition during solidification is given by the equation

$$C_l = C_0/[1 - f_s(1-k)] \qquad [12]$$

where C_l = the concentration of hydrogen in the liquid;
C_0 = the initial concentration of hydrogen in the liquid, prior to solidification;
f_s = the fraction of solid, by weight, in the mushy region; and
k = the distribution coefficient of hydrogen between solid and liquid.

It will be convenient to convert Eq. [12] to one which uses volume fraction of solid by using the conversion relationship

$$f_s = \frac{\rho_s g_s}{\rho_s g_s + \rho_l g_l} = \frac{g_s}{\beta g_s + 1 - \beta} \cong g_s|_{g_s \to 1}$$

We also need to know the partial pressure of hydrogen gas which is in equilibrium with liquid metal having a dissolved hydrogen content, C_l. This is given to us by Sieverts' law and by published solubility data:[18]

$$P_{H_2} = C_P \left(\frac{f_H C_l}{S}\right)^2 = C_p \left(\frac{f_H C_0}{S}\right)^2 \left(\frac{1}{1 - g_s(1-k)}\right)^2 \qquad [13]$$

where C_P = a conversion constant (1×10^5 N · m^{-2}/atm);
f_H = the activity coefficient of hydrogen; and
S = the hydrogen solubility (cm^3/100 g · atm$^{1/2}$).

In pure aluminum, the solubility constant is given by the equation

$$\ln (S) = -5872/T + 6.033 \qquad [14]$$

where T is the thermodynamic (absolute) temperature in degrees Kelvin.

Now we may calculate and compare the hydrodynamic and chemical pressures during the solidification process. Consider how these two pressures change as we move from the riser to the fully solid part of the casting. In the riser, the dissolved gas gives rise to a small chemical pressure, typically on the order of 0.02 to 0.1 atm, and the mechanical pressure is close to 1 atm. (The metallostatic head becomes appreciable in aluminum only in large castings: a height of 1 m produces a head of 0.24 atm.) As we move through the mushy region, the chemical pressure increases because of rejection of gas into the liquid (Eq. [13]), and the mechanical pressure drops because of the flow of liquid through the dendrites (Eq. [11]). It will be thermodynamically possible for porosity to form when the chemical pressure is equal to the mechanical pressure, or when

$$P_{H_2} = P_H^0 \left(\frac{1}{1 - g_s(1-k)}\right)^2 = P_M^0 - \frac{\mu\beta\xi}{(1-\beta)} \frac{8\pi\tau^3}{\gamma^2} \frac{R_x^{5/3} \Delta T}{G_x^{1/3}} \ln \frac{\alpha}{1-g_s} = P_M^0 - B \ln \frac{\alpha}{1-g_s} \qquad [15]$$

where $P_H^0 = C_p(f_H C_0/S)^2$ (the initial gas pressure in the liquid, prior to freezing);
P_M^0 = the mechanical pressure in the riser; and
$B = \frac{\mu\beta\xi}{(1-\beta)} \frac{8\pi\tau^3}{\gamma^2} \frac{R_x^{5/3}\Delta T}{G_x^{1/3}}$

If we divide by P_H^0 in Eq. [15], two dimensionless numbers arise which are of interest, namely,

$$\left(\frac{1}{1 - g_s(1-k)}\right)^2 = \frac{P_M^0}{P_H^0} - \frac{B}{P_H^0} \ln \frac{\alpha}{1-g_s} \qquad [16]$$

The first is the ratio of the mechanical to chemical pressures at the beginning of solidification. The second is the ratio of the B group given by Darcy's law to the

initial chemical (or gas) pressure. When numerical values are placed in this equation (Table I), we find that the chemical pressure of hydrogen overwhelms the B term which arises from Darcy's law. To help visualize this effect, Eqs. [11] and [13] have been plotted together in Figure 5 for A356 (Al-7 pct Si-0.3 pct Mg) alloy. The mechanical pressure is given by the nearly horizontal line at the top of the figure and varies little: from 1.1 atm at the beginning of solidification to 1.04 atm at $g_s = 0.99$, or 99 pct solidified. This small change arises from the fact that B is equal to 900 N/m^2 (or 0.009 atm). On the other hand, the pressures arising from dissolved hydrogen become substantial, even at low gas contents. From these results, we must conclude that the small changes in mechanical pressure, arising from the flow of liquid through the dendritic semisolid region, do not contribute significantly to porosity. The overriding factor in directional solidification is dissolved gas content.

Before continuing, it is necessary to note a number of factors concerning the calculations shown in Figure 5. The activity coefficient of hydrogen, f_H, increases from 1.48 to 1.78 as silicon increases to the eutectic composition during solidification. There is also a temperature drop of 60 °C, which lowers the gas solubility, S, from 0.54 to 0.4. For gas contents normally found in practice, porosity would evolve in or near the eutectic portion of solidification, and consequently, the values of f_H and S at this point are used in the calculations.

The intersection of the curves for mechanical pressure and the chemical pressure of dissolved gas in Figure 5 indicate the point at which porosity formation becomes thermodynamically stable. In other words, the pressure of gas inside a pore must be at least as large as the mechanical pressure of the system; otherwise, the walls of the pore (which is present in liquid) will collapse. It is evident that the fraction solidified at which porosity may form is a direct function of the amount of dissolved gas present at the start of solidification. If the gas content is varied continuously, the intersection of the two curves in Figure 5 generates another curve, which is shown as the baseline in Figure 6. The results are plotted as a function of the dimensionless group, P_H^0/P_M^0. Taken by itself, this curve suggests that porosity depends only on the amount of gas present.

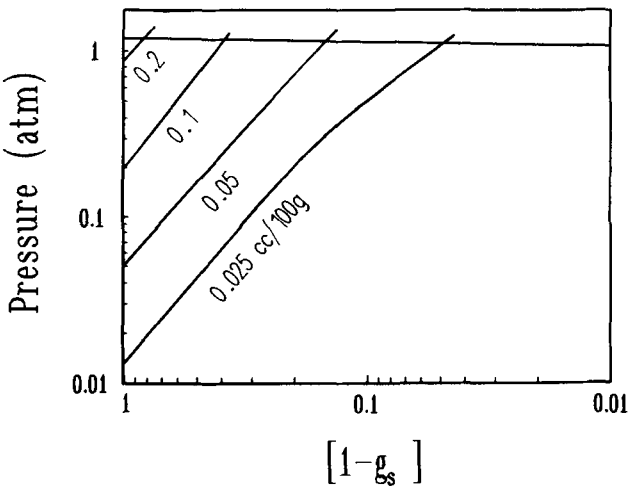

Fig. 5—Plot of the mechanical and chemical pressures during the *directional* solidification of A356 alloy.

Unfortunately, this simple conclusion is not borne out in practice. The amount of porosity formed in directional solidification experiments and in commercial castings decreases with faster solidification rates. The reason for this discrepancy is that we have heretofore ignored the surface tension of the gas-metal interface. The importance of this phenomenon may be illustrated by a simple calculation: The equilibrium surface tension pressure inside a spherical pore, 10 μm in diameter and in liquid aluminum, is 3.6 atm!

We introduce surface tension effects by using the thermodynamic and geometric arguments proposed by Poirier *et al.*[7] The surface tension pressure existing inside small gas bubbles will be

$$P_g - P = \sigma(1/r_1 + 1/r_2) \qquad [17]$$

Table I. Values of Constants Used for Calculations (A356 Alloy Containing 7 Pct Si)

Constant	Value Used in the Calculations	Note
f_H	1.78 ($\log f_H = 0.03 \cdot$ pct Si $- 0.0008 \cdot$ (pct Si)^2)	Ref. 18
S	0.40 (cc/100 g $\cdot$ atm$^{1/2}$)	T_E = 845 K
P_M^0	1.1 atm ($1.1 \cdot 10^5$ N $\cdot$ m^{-2})	—
μ	$1.2 \cdot 10^{-3}$ kg/m $\cdot$ s	Ref. 19
β	0.058	Ref. 8
ξ	1.2	Ref. 13
$8\pi\tau^3$	2700	Ref. 16
γ	$1.15 \cdot 10^{-4}$ m/s$^{1/3}$	Ref. 20*
ΔT	60 °C	Ref. 13
α	0.7 ($\alpha = 1 - f_s^c$)	Refs. 12, 13
G_x	400 °C/m	Ref. 17**
R_x	$8.3 \cdot 10^{-4}$ m/s	Ref. 17**
ρ_s	2550 kg/m^3	Ref. 8
H	433,000 J/kg	Ref. 11
K_M	184 W/m $\cdot$ K	Ref. 11
C_M	1200 J/kg $\cdot$ K	Ref. 21
α	$6 \cdot 10^{-5}$ m^2/s	—

*The primary dendrite arm spacing is assumed to be 2.5 times the secondary arm spacing, as in Al-Cu alloys.[7]
**These values are for a location 2 cm from the end of the plate, where solidification should be directional.

where P_g = pressure inside the gas containing pore;
P = the pressure within the mushy zone;
σ = the surface tension of the liquid; and
r_1, r_2 = the principal radii of curvature of the pore.

For a spherical bubble,

$$P_g - P = 2\sigma/r \qquad [18]$$

where r is the radius of the bubble. Poirier *et al.* considered the conical groove existing between primary dendrites and showed that the width of this groove, δ, at any point in the mushy region depends on the volume fraction of liquid:

$$\delta = g_l d_1/2 \qquad [19]$$

where d_1 is the primary dendrite spacing.* Since $r_1 = \delta/2$ and $r_2 = \infty$ for a cylindrical pore, it follows that

$$P_g - P = 4\sigma/g_l d_1 \qquad [20]$$

Equation [20] is now added to the mechanical pressure in the mushy region. The gas porosity becomes thermodynamically stable when the chemical pressure is equal to, or greater than, the sum of the mechanical and surface tension pressures, namely,

$$P_{H_2} = P_H^0\left(\frac{1}{1 - g_s(1-k)}\right)^2 \geq P_M^0 - B\ln\frac{\alpha}{1-g_s} + \frac{4\sigma}{d_1}\frac{1}{g_l} \qquad [21]$$

As we have seen above, the B term is very small and can be ignored without serious error. That means that we must solve this equation:

$$\left(\frac{1}{1 - g_s(1-k)}\right)^2 = \frac{P_M^0}{P_H^0} + \frac{P_\sigma^0}{P_H^0}\frac{1}{1-g_s} \qquad [22]$$

where $P_\sigma^0 = 4\sigma/d_1$. This represents the additional pressure, caused by surface tension forces, at the beginning of solidification. As the rate of solidification increases, the primary dendrite arm spacing, d_1, decreases. Consequently, any porosity that forms must squeeze into a smaller space, and the pressure caused by surface tension effects, P_σ^0, increases. Rapid solidification therefore makes it more difficult for porosity to form.

Equation [21] is quadratic and has two roots, one of which is physically significant. The meaningful root represents the point at which gas porosity first becomes thermodynamically stable and is called g_s^*. It is plotted in Figure 6 for various values of P_σ^0.

To place the curves in Figure 6 in perspective, it is useful to consider the physical meaning of the different values of the surface tension pressure, P_σ^0. Remembering that the primary arm spacing is related to the cooling rate, for aluminum-based alloys we may calculate the following values:

*Equation 19 has been derived from geometric arguments for a columnar grain structure. For equiaxed grains, another equation has been derived.[8] The relationship for columnar grains has been employed, since the resulting equations are more easily solved.

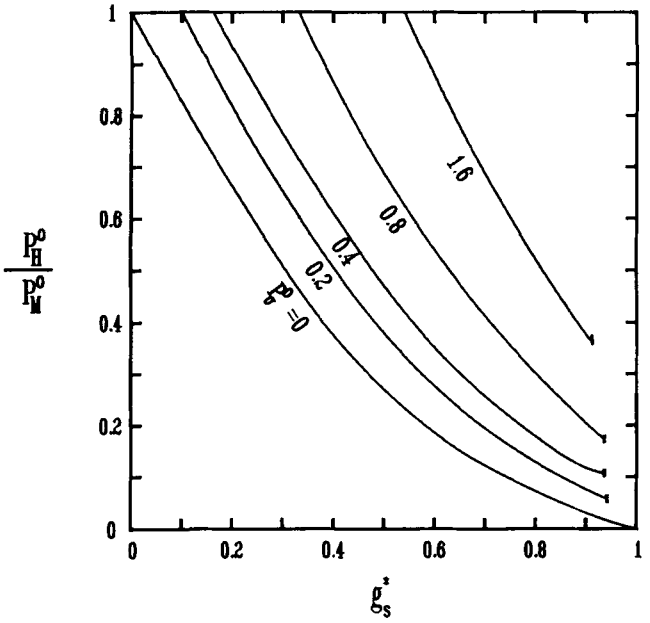

Fig. 6—The fraction solid at which gas formation becomes thermodynamically possible in 356 alloy.

P_σ^0	d_1 (μm)	GR (deg/s)
0	∞	0
0.2	180	0.3
0.4	90	2
0.8	45	17
1.6	23	130

As the cooling rate and P_σ^0 increase, the fraction solidified at which gas porosity may form, g_s^*, also increases. Also note that below a certain small gas content, which depends on solidification rate, no porosity occurs. An analysis of Eq. [22] shows that when $P_\sigma^0/P_H^0 \geq 4$, the pressure of the gas does not increase sufficiently for porosity to form. When this theoretical threshold hydrogen content is compared to the experimental values measured by Fang and Granger[9] (Figure 7), the agreement is seen to be excellent. (In their experiments, no samples exhibited a "zero" porosity, so the threshold hydrogen content was plotted at three small constant fractions of porosity, f_p.)

Taking the data in Figure 6 as a basis for calculation, we can estimate the amount of porosity which may form. Imagine that we have a small volume of solid and liquid, equal to 1 cm^3, which has just reached the point where gas formation is possible. The total volume of liquid left in this volume element is $1 - g_s^*$, and assuming an ideal gas, the volume of hydrogen contained in the liquid, if it were to evolve at the locally prevailing pressure and temperature, is

$$V_g = C_H^0\frac{\rho_l}{100}\frac{T}{273}\frac{1}{P_H^*}\frac{1-g_s^*}{1-g_s^*(1-k)} \qquad [23]$$

The questions now are these: How much of this gas is evolved as porosity, and how much remains trapped in the solid? If we assume that all of the hydrogen which segregates from the solid manages to diffuse to the pore

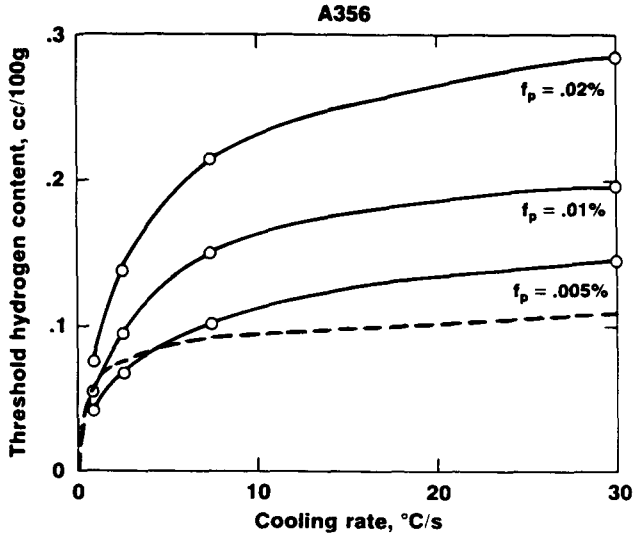

Fig. 7—Threshold hydrogen contents in grain-refined A356 alloy for various porosity levels, from Ref. 9 (solid lines), compared with the theoretical value for zero porosity (from Eq. [22], dashed line).

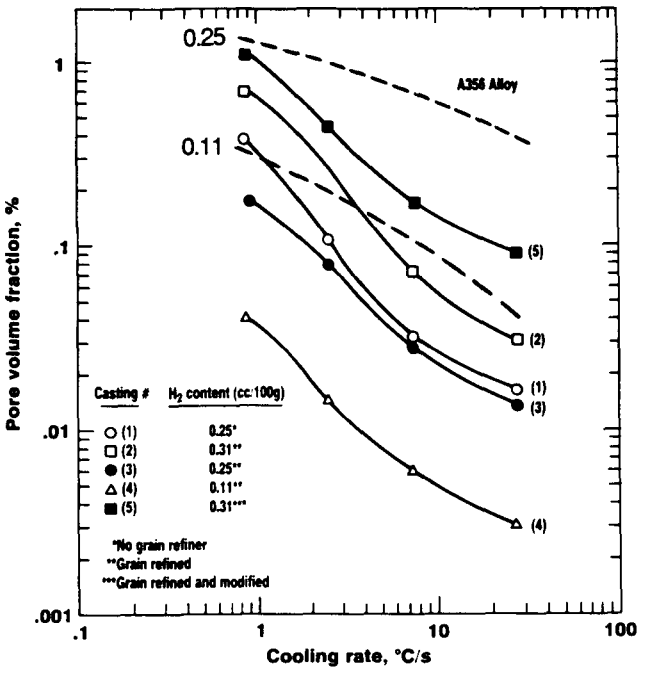

Fig. 8—Pore volume fraction as a function of cooling rate for directionally solidified A356 alloy. (Solid curves are from Ref. 9; dashed curves are theoretical values, Eq. [24].)

(which continues to grow at the thermodynamic equilibrium pressure, P_H^*), then a fraction $(1 - k)$ of the gas given in Eq. [23] will be evolved as porosity. Also, it is desirable to express the porosity formed as a percentage of the total volume of the system. Hence, the volume percentage of porosity becomes

$$V_g^{pct} = C_H^0 \rho_l \frac{T}{273} \frac{1-k}{P_H^*} \frac{(1-g_s^*)}{1-g_s^*(1-k)}$$

$$\cong \frac{7.8 \cdot C_H^0}{P_H^*} \frac{1-g_s^*}{1-g_s^*(1-k)} \qquad [24]$$

at the Al-Si eutectic temperature and composition. The term P_H^* is the pressure inside the gas bubble when it first forms. The last term on the right-hand side of Eq. [24] represents the fraction of gas which is evolved as porosity. (The rest has remained dissolved in the solid.)

The amount of porosity predicted by Eq. [24] and Figure 6 is plotted in Figure 8 with the data provided by Fang and Granger[9] for two initial gas contents, 0.11 and 0.25 cc/100 g. There is a some qualitative agreement between the predicted and observed values, since the lines are nearly parallel, but the theoretical values are too high. This discrepancy may be caused by slow diffusion of hydrogen to the pores, as proposed by Fang and Granger. Lower gas contents and more rapid solidification rates mean that the pores become fewer and further apart, making the diffusion process more difficult, and it is exactly for these cases that the disagreement between theoretical and experimental results (Figure 8) is the worst.

We must also remember that the "thermodynamic" model does not account for gas supersaturation required for pore nucleation. From experimental and theoretical studies,[22,23,24] it is obvious that homogeneous nucleation of a gas bubble in liquid metals is virtually impossible. The internal pressure required (by supersaturation of liquid with dissolved gas) to form the nucleus of critical size is extremely high. Pores therefore form by heterogenous nucleation, usually on oxides. This observation explains why it appears to be possible to "filter out" gas in castings.[25,26] Nucleation effects would tend to delay porosity formation and will have the same effect as increasing the effective surface tension of the metal or increasing the solidification rate. In other words, the porosity is decreased.

In spite of its limitations, the "thermodynamic" approach is valuable. It does predict when porosity may form, and it is possible to account for the pore nucleation and the limited diffusion of gas by introducing a constant, ψ, in Eq. [24]:

$$V_g^{pct} = \frac{C_H^0 \rho_l}{\psi} \frac{T}{273} \frac{1-k}{P_H^*} \frac{(1-g_s^*)}{1-g_s^*(1-k)} \qquad [24a]$$

From the data provided by Fang and Granger,[9] ψ is between 3 and 9 in aluminum alloy castings.

B. *Nondirectional Solidification*

We consider next the important question of feeding distance. This is modeled by the solidification of the plate shown in Figure 9. At the end of the plate, there is no extraction of heat. An insulating wall has been placed at this location in the figure, but it may be easier to produce this situation experimentally by "doubling" the casting. We consider the flow of liquid through the central channel of the plate. To help in visualizing this, consider a slice of unit length taken somewhere from the center of this semi-infinite solid (Figure 10). We assume that the fraction of liquid is a linear function of the distance from the centerline:

$$g_l = g_l^c \left(1 - \frac{y}{l}\right) \qquad [25]$$

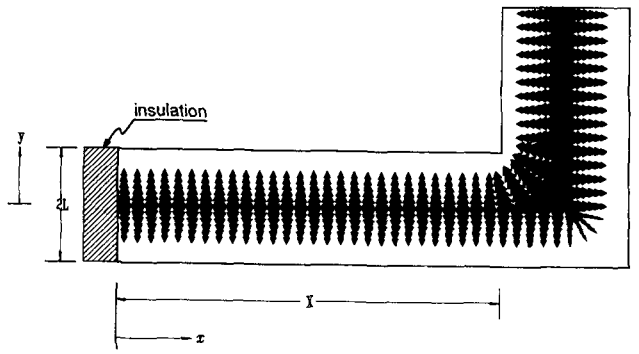

Fig. 9—Schematic illustration of solidification in a semi-infinite plate.

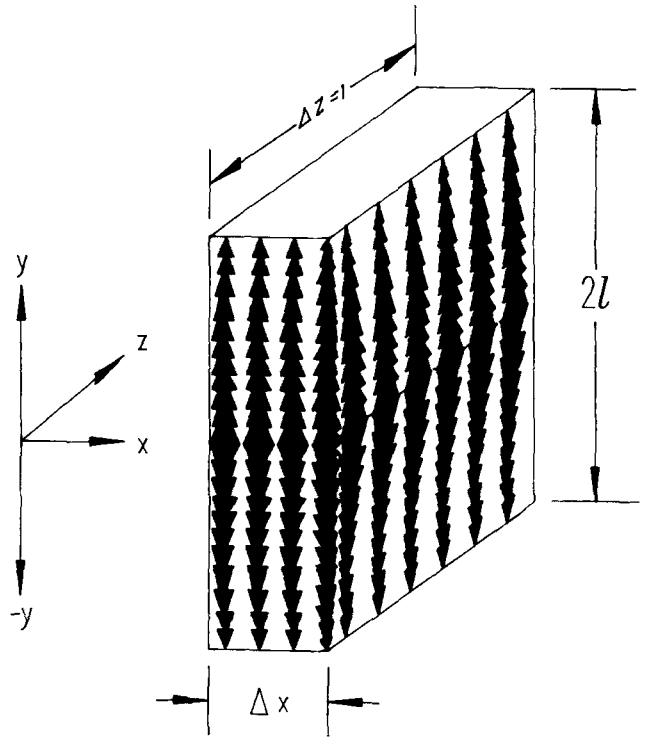

Fig. 10—Volume element taken from the central portion of the plate casting shown in Fig. 9.

where g_l^c is the fraction of liquid at the centerline and can be approximated by the relationship

$$g_l^c = \frac{1}{\xi}\frac{G_y l}{\Delta T} \qquad [26]$$

where ξ is a constant which depends on the alloy being cast. Hence,

$$g_l = \frac{1}{\xi}\frac{G_y l}{\Delta T}\left(1 - \frac{y}{l}\right) \qquad [27]$$

From Darcy's law, we know that the pressure drop across this volume element is related to the total instantaneous flow of liquid through the porous channel. From Eqs. [7] and [8] we find that

$$\nabla P = -\frac{\mu \cdot 8n\pi\tau^3}{g_l} V_l \qquad [28]$$

From the continuity of mass in the system (Eq. [2]), it follows that

$$\nabla \cdot (g_l V_l) = \frac{-\beta}{1-\beta}\frac{\partial g_s}{\partial t} = \frac{-\beta}{1-\beta}\frac{G_y}{\xi \Delta T} R_y \qquad [29]$$

From the geometry of the casting, it is reasonable to assume that R_y is constant and does not depend on the distance, x, along the length of the plate. Then from Eq. [28] we have

$$V_l g_l = \frac{-1}{\mu \cdot 8n\pi\tau^3} g_l^2 \nabla P$$

or

$$\nabla \cdot (V_l g_l) = \frac{-1}{\mu \cdot 8n\pi\tau^3} \nabla(g_l^2 \nabla P)$$

$$= \frac{-1}{\mu \cdot 8n\pi\tau^3} [g_l^2 \nabla^2 P + 2g_l \nabla P \cdot \nabla g_l] \qquad [30]$$

From the shape of the casting, it is obvious that $\partial g_l/\partial x = 0$, and from Eq. [27],

$$\frac{\partial g_l}{\partial y} = \frac{-1}{\xi}\frac{G_y}{\Delta T}$$

Therefore,

$$\nabla \cdot (g_l V_l) = \frac{-1}{\mu \cdot 8n\pi\tau^3}\left(g_l^2 \nabla^2 P - 2g_l \frac{\partial P}{\partial y}\frac{1}{\xi}\frac{G_y}{\Delta T}\right)$$

$$= \frac{-\beta}{1-\beta}\frac{1}{\xi}\frac{G_y}{\Delta T} R_y$$

or

$$\left[g_l^2 \nabla^2 P - 2g_l \frac{\partial P}{\partial y}\frac{1}{\xi}\frac{G_y}{\Delta T}\right] = \mu \cdot 8n\pi\tau^3 \frac{\beta}{1-\beta}\frac{1}{\xi}\frac{G_y}{\Delta T} R_y \qquad [31]$$

Because of symmetry at the centerline, $\partial P/\partial y = 0$. Hence,

$$g_l^2\left\{\frac{\partial^2 P}{\partial y^2} + \frac{\partial^2 P}{\partial x^2}\right\} = \mu \cdot 8n\pi\tau^3 \frac{\beta}{1-\beta}\frac{1}{\xi}\frac{G_y}{\Delta T} R_y \qquad [31a]$$

This expression will be integrated along the centerline to find the liquid pressure as a function of distance from the riser.

$$\frac{\partial^2 P}{\partial y^2} + \frac{\partial^2 P}{\partial x^2} = \frac{\mu \cdot 8n\pi\tau^3}{(g_l)^2}\frac{\beta}{1-\beta}\frac{1}{\xi}\frac{G_y}{\Delta T} R_y$$

$$= \frac{\mu\beta\xi}{1-\beta} 8n\pi\tau^3 \frac{R_y \Delta T}{G_y}\frac{1}{l^2} = \frac{B'}{l^2} \qquad [32]$$

It is of interest to compare the constant B' with the group in Eqs. [11] and [15]. They are the same, except the subscripts of the variables G and R have been changed (to y instead of x). We now assume that $\partial^2 P/\partial y^2$ is zero at the centerline. This may be inferred from the fact that $\partial V_l/\partial y|_{y\to 0} = 0$ and from Darcy's law. (The validity of this assumption is shown in Appendix A, where an alternative method of solution is presented for the plate

casting under consideration.) Equation [32] is now integrated from $x = 0$ to $x = X$, which is the distance from the end of the casting to the riser. The result is

$$P = P_M^0 - \frac{B'}{2} \cdot \frac{X^2}{l^2} \qquad [33]$$

where P_M^0 = the mechanical pressure at the base of the riser;
l = one half the thickness of the inner channel; and
$B' = \dfrac{\mu\beta\xi}{1-\beta} 8n\pi\tau^3 \dfrac{R_y\Delta T}{G_y}$

It should be obvious from Eq. [33] that the pressure will change with time, especially at the end of solidification as the thickness of the inner channel becomes close to zero. In fact, three variables, G, R, and l, change with time. Consequently, an evaluation of the results is easier if we simplify this equation by using a relation given by Flemings[20] for the solidification of sand castings. The thickness of the solidified shell, S, with time is given by*

*We note in passing that Eq. [34] leads to Chvorinov's rule, since $t_c \propto L^2$ and $L \propto V/A$. Thus, even though the equation was derived for solidification of a pure metal having no superheat, it is still a reasonable approximation for steel castings and for alloys having a narrow freezing range.

$$S = \frac{2}{\sqrt{\pi}} \left(\frac{T_m - T_0}{\rho_s H} \right) \sqrt{K_m \rho_m C_m} \sqrt{t} = C' \sqrt{t} \qquad [34]$$

This means that

$$l = L - C' \sqrt{t} \text{ and } R_y = \frac{\partial l}{\partial t} = \frac{C'}{2\sqrt{t}} \qquad [35]$$

To evaluate the physical significance of the above relationship, it is useful to place numerical values into the equation. We first turn once again to the experimental data of Pellini,[1] as well as the later work by Johnson and Loper.[27] The thermal gradient, G_y, was not reported directly by Pellini, but it may be calculated from simple thermal calculations which are given below. The values of the physical constants used are shown in Table II. We consider the 4 inch- (10-cm-) thick casting studied by Pellini. For this casting, the constant B' is equal to 0.00001 atm! This is a very small value, 150 times smaller than the equivalent term calculated above for the directional solidification of A356 alloy. It is interesting to consider the reasons for this. The viscosity of iron is higher than that of aluminum, but the solidification shrinkage, β, is less and nearly balances out the effect of the viscosity. The primary dendrite arm spacing may be estimated from measurements made by Suzuki and co-workers.[20] For the same cooling rate, the dendrite arm spacing in iron is about 3.5 times that found in aluminum. Consequently, for our steel plate, n is less by about a factor of 10. This is one order of magnitude of the decrease in B'. The rest is found in the solidification rate, R, which is nearly a hundred times smaller than before. From the X-rays of porosity in Pellini's plate castings, the shrinkage is found to be on the order of a few millimeters in size. Consequently, the size of the inner liquid channel when shrinkage occurs (and when feeding stops) must also be a few millimeters. We now consider the following values of feeding length, X, predicted from Eq. [33] by assuming that porosity forms (in a gas-free casting) at a distance where the pressure, P, becomes zero:

inner channel size, l	feeding length, X
5 mm	450 cm
1 mm	90 cm

The total observed feeding length for this casting is 45 cm, whereas the theoretical value from Eq. [33] is several times greater.

We must also consider that Eq. [33] is for the idealized case of the semi-infinite plate, where no thermal gradient exists in the feeding (x) direction. Pellini[1] observed shrinkage porosity in his castings whenever the thermal gradient was less than a small critical value, so for all practical purposes, the feeding length in a truly semi-infinite region is very small, perhaps 5 or 10 cm at most. This means that the feeding length predicted by Eq. [33] is too large by 5 to 10 times.

This is not the only problem with the theoretical result. If Eq. [33] is reduced still further, it is possible to estimate how the feeding length changes as we move from steel to aluminum alloy castings. (See Appendix B.) The predicted trends go in the wrong direction!

If we cannot apply Darcy's law to the case of solidification shrinkage, what is the controlling factor? We suggest that the important factor is a "geometric" one, related to the thermal gradient in the feeding direction. In Figure 9, we represented the solidification of a plate in a highly idealized fashion. In practice, one could expect local variations to exist in the freezing rate. These may be caused by

(1) variations in moisture content or density of the sand mold or variation in coating thickness in metal molds;
(2) uneven contraction of the casting away from the mold wall, which causes uneven heat transfer; or
(3) normal variations in the morphology of the solid-liquid interface (see, for example, Figure 4 of Reference 28).

The situation is expressed schematically in Figure 11, where uneven solidification has "pinched off" certain areas, which solidify without feeding, to exhibit shrinkage. The presence of a gradient in the feeding direction serves to open up this channel, by effectively providing a taper to the inner liquid channel. This situation is illustrated in Figure 12.

The tapered channel may be characterized by the angle θ. Let us assume that feeding will occur as long as this angle is greater than a certain critical angle, θ_c. This means that

$$\frac{R_x}{R_y} \geq \tan \theta_c \qquad [36]$$

The value of R_y is given by Eq. [35]. Substituting this in the above equation, we find

$$R_x \geq \frac{C'}{2} \tan \theta_c \frac{1}{\sqrt{t_c}}$$

Table II. Values of Constants Used for Calculations of Feeding Length in a 4-Inch-Thick Steel Casting

Constant	Value Used in the Calculations	Note
P_M^0	1.1 atm ($1.1 \cdot 10^5$ N · m^{-2})	—
μ	$6.2 \cdot 10^{-3}$ kg/m · s	Ref. 11
β	0.038	Ref. 2
ξ	1	—
$8\pi\tau^3$	2700	Ref. 16
γ	$3.8 \cdot 10^{-4}$ m/s$^{1/3}$	Ref. 20*
n	$7.1 \cdot 10^6$/m^2	Ref. 20*
ΔT	45 °C (0.3 pct C steel)	Ref. 1
ρ_s	7500 kg/m^3	Ref. 2
H	270,000 J/kg	Ref. 11
K_M	33 W/m · K	Ref. 6
C_M	315 J/kg · K	Ref. 2
α	$1.4 \cdot 10^{-5}$ m^2/s	—
$G_y R_y$	0.018 C/s	Ref. 1
G_y	240 C/m	Ref. 1
R_y	$7.6 \cdot 10^{-6}$ m/s	Eq. [35]
C'	$8.7 \cdot 10^{-4}$ m/s$^{1/2}$	Ref. 2
K_m	1.58 W/m · K	Ref. 2
ρ_m	1490 kg/m^3	Ref. 2
C_m	530 J/kg · K	Ref. 2

*The primary dendrite arm spacing is assumed to be 2.5 times the secondary arm spacing.

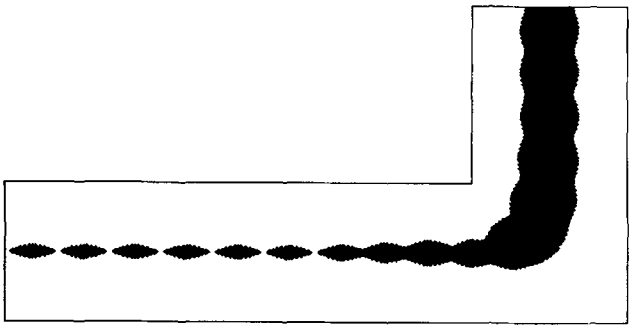

Fig. 11—Cross section of a plate casting which has no thermal gradient in the feeding direction on the left side of the casting. Uneven freezing has left isolated pools which exhibit shrinkage after freezing.

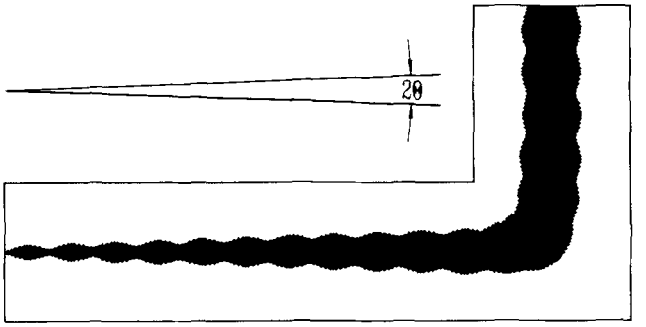

Fig. 12—Cross section of a plate casting where a thermal gradient in the feeding direction creates a tapered liquid pool in the center, which may feed the casting. No shrinkage occurs.

It is possible to show (see the discussion leading to the derivation of Eq. [B5] in Appendix B) that the average gradient in the solid-liquid region is

$$G_x \cong \frac{\rho_s H R_x}{2K_M} \qquad [37]$$

Therefore,

$$G_x \geq \frac{\rho_s H}{2K_M}\frac{C'}{2}\tan\theta_c \frac{1}{\sqrt{t_c}}$$

$$\geq \frac{T_m - T_0}{2\sqrt{\pi K_m}} \cdot \sqrt{K_m \rho_m C_m} \cdot \tan\theta_c \frac{1}{\sqrt{t_c}} = \frac{A}{\sqrt{t_c}} \qquad [38]$$

By placing the appropriate values of the physical constants in this equation (see Table II) and assuming that θ_c is equal to 1 deg, we find that $G_x \geq 30/\sqrt{t_c}$ when the solidification time, t_c, is given in minutes. (Remember that G is in units of K/m.) If we compare this equation with the curve in Figure 2 and ignore for the moment the difference in units, we find that it falls *exactly* on top of the solid line in Figure 2.

The logic of Darcy's law has been so compelling that it has seduced us for some 20 or more years. Even Niyama *et al.*[4] tried to make it explain their results. But Darcy's law does not explain the formation of shrinkage porosity in steel castings, even though it probably applies. The apparent explanation, a simple geometric criterion for the shape of the mushy region, was overlooked.

It is of interest to examine some of the logical implications of Eq. [38] and to compare the predictions with the available data. As noted above, Pellini[2] found that gradients of 0.2 °C to 0.4 °C/cm (or 20 to 40 K/m) were required to prevent shrinkage formation in a 5-cm-thick plate. The freezing time for this plate was 14 minutes, so from Eq. [38] and assuming an angle of 1 deg, the predicted gradient is 8 K/m, which is reasonably close. Or looking at the data in another way, Pellini's data and Eq. [38] suggest that θ_c for steel plates is between 2.5 and 5 deg. This result is certainly reasonable and lends some credence to the approach.

Pellini[2] also reported that for a 10-cm-thick bar casting (for which the solidification time was 17 minutes), the critical temperature gradient was between 1.2 °C and 2.4 °C/cm (120 °C and 240 °C/m). From this result and Eq. [38], the angle of the liquid channel, θ_c, is between 16 and 30 deg. This also appears to be a reasonable result and is a prediction that could be easily verified. One could cast fairly large steel bars and, after partial solidification, replace the remaining liquid by pouring lead into the casting. A more elegant solution, although somewhat more difficult to accomplish experimentally, is to quench and "freeze in" the solid-liquid interface.

It is now possible to reconsider the results of Niyama *et al.*[4] as shown in Figure 2. Their results are for cylindrical bar castings, which should solidify very much like the rectangular bars used by Pellini[1,2] in his study. For the 10-inch bar casting studied by Pellini, Figure 13 predicts a gradient of 7 °C/cm (or 700 °C/m), which is 3 to 6 times greater than the value measured by Pellini by placing thermocouples in his molds. Part of the reason for this discrepency is the fact that Niyama *et al.* defined the gradient as that existing in the fully solid region. Because latent heat is released in the semisolid region, the average thermal gradient in the mushy zone will be less by a factor of 2 (see Appendix B). Since this is the value measured by Pellini and predicted by Eq. [38], this value is drawn in Figure 2 with a dashed line. We should also point out that the gradients shown in Figure 2 have not been measured but were calculated by numerical analysis on a computer. Consequently, the absolute values would depend upon the values of physical constants used in the calculations (especially the thermal properties of the sand). The form of the curve *vs* total solidification time (that is, a straight line *vs* log t_c) is not, however, affected by the value of physical constants used.

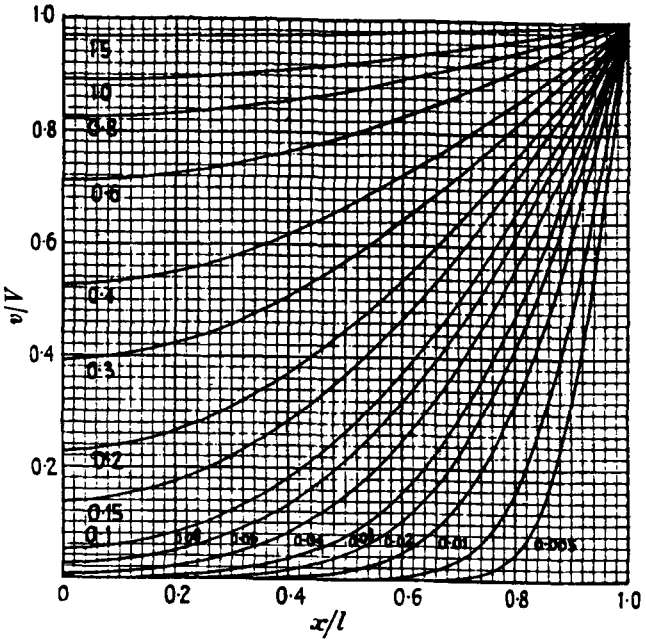

Fig. 13—Temperature distribution at various times in the slab $-1 \leq x \leq 1$ with zero initial temperature and surface temperature V. The numbers on the curve are the values of at/l^2.[29]

Although Eq. [38] was derived for sand castings, it may also apply to metal mold castings. Noting that, for a steel mold, the factor $K_m\rho_mC_m$ will be nearly 100 times greater than for sand, the required gradient for feeding (which is proportional to the square root of $K_m\rho_mC_m$) will be about 10 times greater than the same sand casting.

It is also interesting to consider the feeding of other metals. To take an extreme case, consider the gradient required for aluminum alloy castings. Because of the lower melting point and much higher thermal conductivity, the thermal gradient required for feeding (assuming that θ_c is unchanged) is only 1/12 that for steel castings. This is an interesting prediction, one that could be easily tested in bar castings. The experimental measurement would represent an important test for the "geometric" model.

The experiments in aluminum would be important for another reason. The mode of solidification is quite different. A well-defined shell of solid is less likely to form in aluminum, and the entire casting would quickly fill with dendrites and liquid. This is particularly so of alloys having a very wide freezing range, such as the 200 series of alloys (Al-4.5 pct Cu). Especially in this case, the morphology of the mushy dendritic region would be such that flow of liquid, as envisioned by Darcy's law, would be important for feeding. Consequently, careful experiments in aluminum alloys would establish whether the "geometric" model has a wide range of validity or whether it breaks down as the solidifcation structure changes.

It should also be noted that there is an alternative form of Eq. [38], one that would be more convenient for computer modeling of solidification.

$$\frac{G_x}{R_y} \geq \frac{\rho_s H}{2K_M} \tan\theta_c = A' \tan\theta_c \qquad [38a]$$

The constant A' is equal to 3.0×10^6 C/m$^2 \cdot$ s for aluminum and 3.1×10^7 for steel: 10 times greater than aluminum.

A number of rules have been derived from Eq. [38], and it will be interesting to test their validity experimentally in the future. But, for now, let us turn to the controlling factor in feeding: the thermal gradient in the feeding direction, G_x. What is it that controls this gradient? If the above rules are meaningful, then a prediction of feeding and feeding length, must be related directly to whatever is controlling the gradient. One way to characterize the situation is to consider the analytical solution proposed by Carslaw and Jaeger[29] for a slab $-l \leq x \leq l$ with zero initial temperature and surface temperature V. The dimensionless temperature, v/V, as a function of distance in the slab (or plate) is plotted in Figure 13. The curves are plotted for different values of dimensionless time, $\alpha t/l^2$, where α is the thermal diffusivity of the metal ($\alpha = K_M/\rho_sC_M$). For values of $\alpha t/l^2$ less than about 0.1, the center of the slab does not "see" the effect of the ends. This would correspond to a plate casting that is so long that the central portion develops a central "semi-infinite" section, where shrinkage porosity will occur (and where G_x will be zero). In other words, if we wish to avoid shrinkage porosity, $\alpha t/l^2 \geq 0.1$ or $l^2 \leq 10\alpha t$. To use this equation, we must decide what value is appropriate for the time. It is logical to assume that the total solidification time, t_c, as given by Eq. [35],

is the relevant parameter. In other words, the plate casting must be short enough so that the end effects are felt in the middle of the casting, prior to solidification. It therefore follows that

$$l^2 \leq \frac{10\alpha L^2}{(C')^2} \quad \text{or} \quad \frac{l}{T} \leq \frac{\sqrt{2.5 \cdot \alpha}}{C'} \qquad [39]$$

where l now represents the feeding distance and T $(=2L)$ is the thickness of the casting. If Eq. [39] is used to calculate the feeding distance, l/T, the result for steel plates is 7 and for aluminum plates is 18 *vs* the experimently determined values of 4.5 to 5[1,11,27] and 10 to 15.[11] The calculated values are somewhat too high, but when one considers the simplifications made in the above analysis, the agreement may be considered to be excellent. In any event, the purpose is to illustrate what controls the gradient, G_x, during solidification. It can be seen that the geometry of the mold and the thermal diffusivity of the metal are most important.

A more accurate prediction may be made by the use of Eq. [38a] and numerical analysis to calculate the temperature gradient during solidification. This approach also becomes necessary when the geometry is complicated. Even the analysis of the feeding of a simple bar casting is quite complex, and the use of a computer may be easier even in this simple case.

In the above analysis, we assumed that shrinkage occurred suddenly when the angle of the thermal taper reached a critical value, θ_c. In practice, the amount of shrinkage porosity present could be expected to depend on the value of the taper, once the angle is less than θ_c. This may be illustrated by considering the early experiments of Campbell,[30] whose results for cobalt and steel bars are reproduced in Figure 14. When the angle of the taper is greater than a certain value, the level of porosity is constant. This porosity level depends on dissolved gas content and freezing rate, as discussed above under the "thermodynamic" model. As the angle becomes less than the critical value, about 2 to 3 deg in these castings, the porosity increases gradually, to a maximum at 0 deg. (Please note that the angle of the taper will generally not be equal to the angle of the inner feed channel, θ.) A similar behavior in A356 alloy castings may be inferred from the results of Lee *et al.*[17] (Figure 15). As shown above, G_x/R_y is proportional to the tangent of the angle of the thermal taper. Lee *et al.* did not specify what G and R were plotted in their figure, but from the geometry of their plate castings, it is probable that their results show the ratio of G_x/R_y multiplied by the local solidification time to the two-thirds power. This latter factor can be expected to vary little along the length of their plates, so their results are, for all practical purposes, a plot of porosity *vs* G_x/R_y.

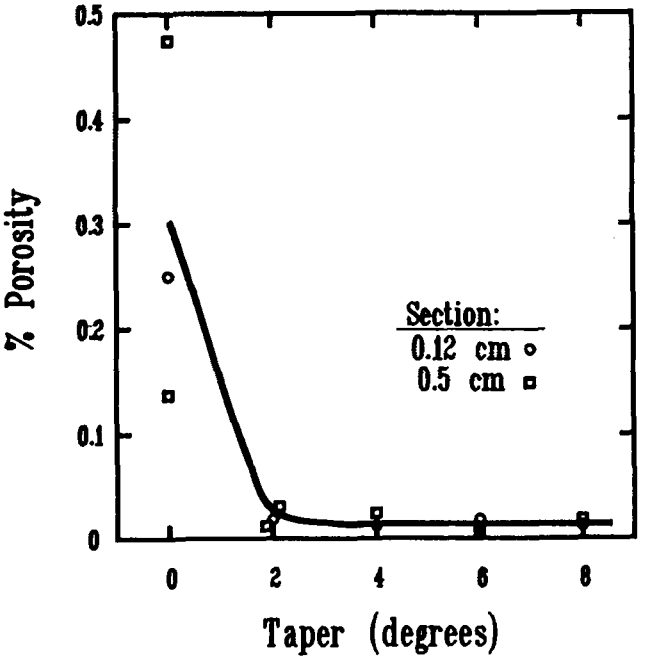

(*a*)

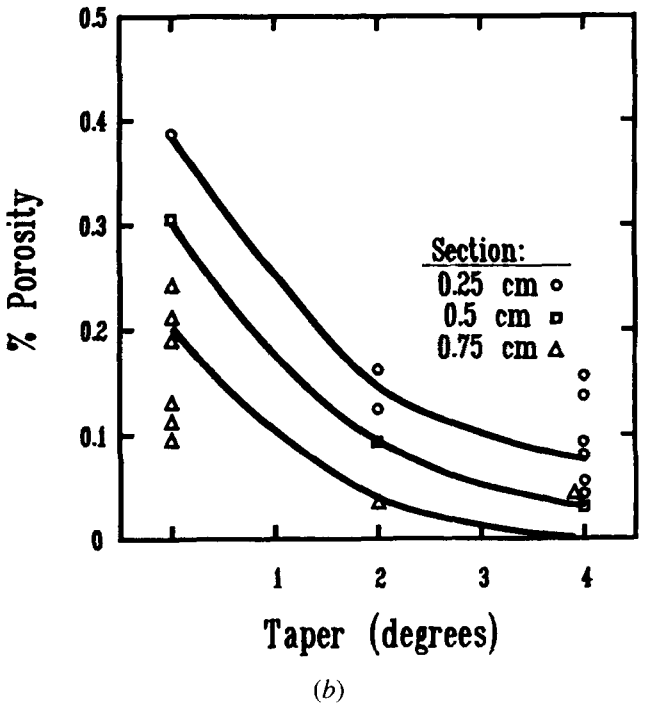

(*b*)

Fig. 14—The effect of taper on porosity in bar castings of (*a*) iron-0.25 pct C and (*b*) cobalt-based alloys.[30]

III. CONCLUDING REMARKS

The theoretical analyses in this article suggest a number of useful experiments. It would be particularly interesting to study the feeding of aluminum alloy castings in detail, in order to compare the results to those found in steel. Also, a relationship similar to that plotted in Figure 2, but for aluminum, would determine the range of validity of the "geometrical" feeding criterion presented in Eq. [38]. It would also be of interest to measure the angle of the inner feed channel in steel castings and compare it to that predicted from the theory.

It may also be interesting to do experiments at increased pressures. In the absence of shrinkage, the amount of porosity could be expected to depend on pressure, as suggested by Eq. [24].

Some useful work may also be done by incorporating

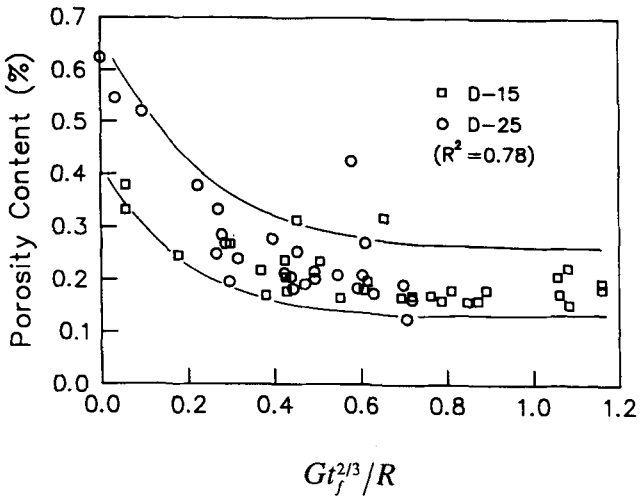

Fig. 15—Porosity distribution in A356 alloy plate castings.[17]

the models proposed here into existing finite element model programs, in order to theoretically predict porosity levels reported in published work or found in commercial castings. This would be another way to test the validity of the models proposed in this study.

NOMENCLATURE

A	$\frac{T_m - T_0}{2\sqrt{\pi}K_M} \cdot \sqrt{K_m\rho_m C_m}$
A'	$\frac{\rho_s H}{2K_M}$
B	$\frac{\mu\beta\xi}{(1-\beta)} \frac{8\pi\tau^3}{\gamma^2} \frac{R_x^{5/3}\Delta T}{G_x^{1/3}}$
B'	$\frac{\mu\beta\xi}{1-\beta} 8n\pi\tau^3 \frac{R_y\Delta T}{G_y}$
C'	$\frac{2}{\sqrt{\pi}} \left(\frac{T_m - T_0}{\rho_s H}\right) \sqrt{K_m\rho_m C_m}$
C_l	concentration of hydrogen in the liquid
C_0	initial concentration of hydrogen in the liquid, prior to solidification
C_m	specific heat of the mold
d_1	primary dendrite spacing
d_2	secondary dendrite arm spacing
f_H	activity coefficient of hydrogen in liquid metal
f_p	volume fraction of porosity, in Figure 7
f_s	fraction solid by weight in the mushy region
f_s^c	fraction solid at which dendrite coherency occurs and where mass feeding stops
g	gravitational constant
g_l	volume fraction liquid at the point under consideration
g_s	volume fraction solid at the point under consideration
g_s^*	volume fraction solid at which porosity becomes thermodynamically stable and may form
G	thermal gradient at any point inside the casting (°C/m)
H	latent heat of fusion of the metal or alloy
k	distribution coefficient of hydrogen between solid and liquid
K	specific permeability of the solid dendrites in the mushy region
K_m	thermal conductivity of the mold
K_M	thermal conductivity of the metal
l	length of the mushy region in the casting; also one half the thickness of the liquid channel, along the center of a solidifying plate casting
L	one half the thickness of a plate casting
n	number of flow channels per unit area
P	mechanical or hydrostatic pressure at any point under consideration
ΔP	pressure drop along the length of the casting
P_g	pressure inside a gas-containing pore
P_{H_2}	effective (chemical) pressure of hydrogen dissolved in the liquid metal
P_H^0	$C_p(f_H C_0/S)^2$, the initial gas pressure in the liquid, prior to solidification
P_H^*	pressure inside the gas bubble when it first forms
P_M^0	mechanical pressure in the riser
P_σ^0	$4\sigma/d_1$, the additional pressure, caused by surface tension forces, at the beginning of solidification
r	the radius of curvature of a spherical pore
r_1, r_2	the principal radii of curvature of the pore
R	solidification velocity in the casting (m/s)
S	solubility constant for hydrogen in liquid metal; also the thickness of a solidified shell in Eq. [34]
t	time (s)
t_c	time for the casting to become fully solid at the centerline
t_f	local solidification time
T	thickness of the plate casting; also the temperature
T_l	liquidus temperature of the alloy
T_m	melting point of a (pure) metal in Eq. [34]
T_0	temperature of the mold prior to casting
T_s	solidus temperature of the alloy
ΔT	freezing range of the alloy ($T_l - T_s$)
V_g	volume fraction of gas porosity
V_g^{pct}	volume percentage of gas porosity
V_l	linear flow velocity of liquid
V_x	linear flow velocity of liquid in the x-direction
x	distance along the length of a casting
X	length of a casting (distance from the end of the casting to the riser)
y	elevation or height from the centerline of a casting
α	fraction of the solid-liquid region where mass feeding does not occur; also $\alpha = K_M/\rho_s C_M$, the thermal diffusivity of the metal
β	solidification shrinkage factor, $(\rho_s - \rho_l)/\rho_s$
γ	an empirical constant which relates primary dendrite arm spacing to local solidification time

δ width of the interdendritic groove at any point in the mushy region
θ angle of the liquid feeding channel inside a casting
θ_c critical angle below which shrinkage porosity occurs
λ portion of the liquid-solid region where liquid must flow between a skeleton of interlocking solid dendrites
μ viscosity of the liquid
ξ dimensionless constant which corrects for a nonlinear dependence of f_s with temperature during solidification
ρ_l density of liquid metal at its freezing point
ρ_m density of the mold
ρ_s density of the solid metal
σ surface tension of the liquid
τ tortuosity of the flow channels in the interdendritic region
τ_s t/t_c, a dimensionless solidification time
ϕ $(1 - \sqrt{\tau_s})\sqrt[4]{t_s} \cong 1 - \sqrt{\tau_s}$

APPENDIX A

An alternative derivation

An alternative solution for the pressure distribution in a semi-infinite slab is given below. From the continuity equation, we have

$$\nabla \cdot (g_l \bar{V}) = \frac{-\beta}{1-\beta}\frac{\partial g_s}{\partial t} = g_l\left(\frac{\partial V_x}{\partial x} + \frac{\partial V_y}{\partial y}\right) + V_x\frac{\partial g_l}{\partial x} + V_y\frac{\partial g_l}{\partial_y} \quad [A1]$$

From our assumed geometry, we find that $\partial g_l/\partial x = 0$. Let us assume that the temperature in the center channel ($-l \le y \le l$) is of the form

$$T - T_s = -\frac{G^0 l}{2}\left[1 - \left(\frac{y}{l}\right)^2\right] \quad [A2]$$

where $G^0 = \left.\frac{\partial T}{\partial y}\right|_{y \to l^+}$

The fraction liquid will be proportional to $T - T_s$ and inversely proportional to the freezing range, or

$$g_l = -\frac{G^0 l}{\xi 2\Delta T}\left[1 - \left(\frac{y}{l}\right)^2\right] \quad [A3]$$

from which $\frac{\partial g_l}{\partial y} = \frac{G^0}{\xi \Delta T}\frac{y}{l}$

Because $g_s = 1 - g_l$, we also find from Eq. [A3] that

$$\frac{\partial g_s}{\partial t} = -\frac{\partial g_l}{\partial t} = -\frac{\partial g_l}{\partial l}R = \frac{G^0}{\xi 2\Delta T}R\left[1 + \left(\frac{y}{l}\right)^2\right] \quad [A4]$$

We now combine Eqs. [A1], [3], and [4]:

$$\frac{-\beta}{1-\beta}\frac{G^0}{\xi 2\Delta T}R\left[1 + \left(\frac{y}{l}\right)^2\right] = -\frac{G^0 l}{\xi 2\Delta T}\left[1 - \left(\frac{y}{l}\right)^2\right] \cdot \left(\frac{\partial \bar{V}}{\partial x} + \frac{\partial \bar{V}}{\partial y}\right) + \bar{V}\frac{G^0}{\xi \Delta T}\frac{y}{l} \quad [A5]$$

At the centerline, this equation reduces to

$$\frac{\partial \bar{V}}{\partial x} + \frac{\partial \bar{V}}{\partial y} \cong \frac{\partial \bar{V}}{\partial x} = \frac{-\beta}{1-\beta}\frac{R}{l} \quad [A6]$$

We now place this value into the differential form of Darcy's law:

$$\frac{\partial P}{\partial x} = \frac{\mu}{g_l} 8n\pi\tau^3 \bar{V}_x = \frac{-\mu\beta\xi}{1-\beta} 8n\pi\tau^3 \frac{\Delta T R_y}{G_0}\frac{x}{2l^2} \quad [A7]$$

This may be integrated to yield Eq. [42] and is exactly the same result as obtained before, except that the definition of the gradient, G_0, is defined differently and more exactly. This means that the result is of general validity and is not sensitive to the assumed temperature profile or profile of g_s. This result is not surprising, since the overall driving force for fluid flow is solidification shrinkage. As material freezes, it shrinks, and liquid must flow for feeding to occur. The pressure drop described by Darcy's law arises from this flow. That this is the case should be clearer from the above derivation.

APPENDIX B

Calculation of feeding lengths from Darcy's law

It is convenient to define a dimensionless solidification time, $\tau_s = t/t_c$, where t_c is the total time it takes for the casting to freeze at the centerline. The pressure at the centerline of the casting (Eq. [33]) now becomes

$$P = P_M^0 - \frac{\mu\beta\xi}{1-\beta} 8n\pi\tau^3 \frac{\Delta T}{G_y} \cdot \frac{1}{t_c L} \cdot \frac{1}{(1-\sqrt{\tau_s})^2 4\sqrt{\tau_s}} \cdot X^2 \quad [B1]$$

From Pellini's experimental results[2] it would appear that $G_y = G^0/L$, where G^0 is equal to 115 °C in his steel plates. Equation [B1] becomes

$$P = P_M^0 - \frac{\mu\beta\xi}{1-\beta} 8n\pi\tau^3 \frac{\Delta T}{G^0} \cdot \frac{(C')^2}{(1-\sqrt{\tau_s})^2 4\sqrt{\tau_s}} \cdot \frac{X^2}{L^2} \quad [B2]$$

Equation [B2] may be reduced still further by considering what controls the temperature gradient in the two-phase mushy zone. The heat of fusion is released throughout this region, much as heat would be generated by an electric current. This "dispersed" heat of fusion must pass through the solid-liquid region by conduction to the fully solid shell and then to the mold. If we assume that the release of latent heat of fusion is proportional to the fraction solid and distance in the two-phase

region and further assume that the thermal conductivities of solid and liquid are equal, then it follows that the temperature gradient in the mushy region is

$$\frac{\partial T}{\partial y} = \frac{1}{K_M}\left(1 - \frac{y}{l}\right)\rho_s H R_y \qquad [B3]$$

where K_M is the thermal conductivity of the metal (the uppercase M represents the metal; the lowercase m represents the mold) and where l represents the total length of the mushy zone. The position inside the mushy zone is given by y. Integrating Eq. [B3], we find that

$$T = \frac{\rho_s H R_y}{K_M}\left(y - \frac{y^2}{2l}\right) + T_s \qquad [B4]$$

and at the end of the mushy zone, where $y = l$ and $T = T_l$,

$$T_l - T_s = \frac{\rho_s H R_y}{K_M}\left(l - \frac{l^2}{2l}\right)$$

The average gradient in the solid-liquid region is given by

$$G_y \cong \frac{T_l - T_s}{l} = \frac{\rho_s H R_y}{2K_M} \qquad [B5]$$

We now find R_y from Eq. [35]. At the end of solidification (that is, at $t = t_c$), the desired result is

$$G_y \cong \frac{\rho_s H}{4K_M}\cdot\frac{(C')^2}{L} = \frac{G^0}{L} \qquad [B6]$$

We may now place Eq. [B6] in Eq. [B2] to obtain

$$P = P_M^0 - \frac{\mu\beta\xi}{1-\beta} 8n\pi\tau^3\Delta T\cdot\frac{4K_M}{\rho_s H} \cdot\frac{1}{(1-\sqrt{\tau_s})^2 4\sqrt{\tau_s}}\cdot\frac{X^2}{L^2} \qquad [B7]$$

This is the reduced form of the equation for feeding length along the centerline of plate castings. From a physical point of view, it is reasonable to assume that centerline porosity will result when the mechanical pressure, P, assumes a zero or negative value. In the presence of dissolved gas, porosity may occur at higher pressures, but we shall ignore this for the time being and set P equal to zero. Also remember that the number of flow channels is inversely proportional to the primary dendrite arm spacing. From available data[20] on dendrite arm spacings in aluminum- and iron-based alloys, we find that

$$d_1 \cong \gamma(GR)^{-1/3}$$

Substituting in Eq. [B7] and rearranging, we find that

$$\frac{X}{L} = \phi\gamma(GR)^{-1/3}\sqrt{P_M^0\frac{1-\beta}{\mu\beta\xi}\cdot\frac{1}{8\pi\tau^3}\cdot\frac{1}{\Delta T}\cdot\frac{\rho_s H}{K_m}} \qquad [B8]$$

where $\phi = (1-\sqrt{\tau_s})\sqrt[4]{\tau_s} \cong 1 - \sqrt{\tau_s}$

It would appear from Eq. [B8] that the feeding length, X/L, is a weak function of cooling rate, not a constant ratio, as suggested by Pellini.[1,2] This is the first problem with the equation. A second problem is that the equation predicts the feeding length will increase with the square root of pressure at the base of the riser, whereas Pellini observed that there was not an appreciable effect of increased pressure. The final and most serious problem is revealed by comparing the experimental and theoretical feeding lengths for steel and aluminum plates.[11] We could, for example, take X/L in steel plates to be 9 to 10, as measured by Pellini and others,[1,11] and then calculate the value of ϕ which falls out of the equation. This can then be treated as an empirical constant. Now we place this value for ϕ along with the appropriate numerical values of the physical constants for aluminum (Table I) and find that X/L in an aluminum alloy plate should be about 1, or one tenth of the feeding distance found in steel. This is because

(1) γ is about 3.5 times smaller. This "tighter" structure restricts the flow of liquid.
(2) The thermal conductivity of Al is five times, and the effective latent heat ($\rho_s H$) is one half that of steel.

From the experimental data of Davies,[11] we find that the feeding length, X/L, increases to about 20, instead of decreasing to about 1, as predicted by Eq. [B8]. In other words, Darcy's law does not apply to the calculation of feeding lengths. We must seek another mechanism for the formation of shrinkage porosity.

Darcy's law cannot be invoked to explain feeding lengths because the liquid velocities found during solidification are small. The total volume of liquid shrinkage is only a few percent of the total volume, and in the case of our 4-inch- (10-cm-) thick steel plate casting, the flow occurs over nearly an hour. The pressure drop associated with the liquid flow is consequently much smaller than the prevailing atmospheric pressure and cannot be responsible for shrinkage porosity.

ACKNOWLEDGMENTS

This work was conducted at the National Center for Excellence in Metalworking Technology. The NCEMT is operated by Concurrent Technologies Corporation (formerly Metalworking Technology, Inc.) under contract to the United States Navy as part of the United States Navy Manufacturing Technology Program.

REFERENCES

1. W.S. Pellini: *Am. Foundrymen's Soc. Trans.*, 1953, vol. 61, pp. 61-80.
2. W.S. Pellini: *Am. Foundrymen's Soc. Trans.*, 1953, vol. 61, pp. 603-22.
3. E. Niyama, T. Uchida, M. Morikawa, and S. Saito: *Am. Foundrymen's Soc. Int. Cast Met. J.*, 1981, vol. 6 (2), pp. 16-22.
4. E. Niyama, T. Uchida, M. Morikawa, and S. Saito: *Am. Foundrymen's Soc. Int. Cast Met. J.*, 1982, vol. 7 (3), pp. 52-63.
5. G.K. Sigworth and C. Wang: *Am. Foundrymen's Soc. Trans.*, 1992, vol. 100, pp. 979-87.
6. K. Kubo and R.D. Pehlke: *Metall. Trans. B*, 1985, vol. 16B, pp. 359-66.
7. D.R. Poirier, K. Yeum, and A.L. Maples: *Metall. Trans. A*, 1987, vol. 18A, pp. 1979-87.
8. K. Yeum and D.R. Poirier: *Light Metals 1988*, TMS, Warrendale, PA, 1988, pp. 469-76.

9. Q.T. Fang and D.A. Granger: *Am. Foundrymen's Soc. Trans.*, 1989, vol. 97, pp. 989-1000
10. Q.T. Fang, P.N. Analebechi, and D.A. Granger: *Light Metals 1988*, TMS, Warrendale, PA, 1987, pp. 477-86.
11. V. de L. Davies: *Am. Foundrymen's Soc. Cast Met. Res. J.*, 1975, vol. 11, pp. 33-44.
12. L. Backerud and G. Chai: University of Stockholm, Stockholm, Sweden, private communication, 1991.
13. L. Backerud, G. Chai, and J. Tamminen: *Solidification Characteristics of Aluminum Alloys*, A.F.S., Des Plaines, IL, 1990, p. 131.
14. M.C. Flemings: *Metall. Trans. B*, 1991, vol. 22B, pp. 269-93.
15. T.S. Piwonka and Flemings: *Trans. TMS-AIME*, 1966, vol. 236, pp. 1157-65.
16. D.R. Poirier: *Metall. Trans. B*, 1987, vol. 18B, pp. 245-55.
17. Y.W. Lee, E. Chang, and C.F. Chieu: *Metall. Trans. B*, 1990, vol. 21B, pp. 715-22.
18. G.K. Sigworth and T.A. Engh: *Metall. Trans. B*, 1982, vol. 13B, pp. 447-60.
19. S. Ganeson, R. Speiser, and D.R. Poirier: *Metall. Trans. B*, 1987, vol. 18B, pp. 421-24.
20. M.C. Flemings: *Solidification Processing*, McGraw Hill, New York, NY, 1974, pp. 12 and 146-54.
21. L.F. Mondolfo: *Aluminum Alloys: Structure and Properties*, Butterworth's, London, 1976, p. 60.
22. J. Campbell: *Castings*, Butterworth-Heinemann Ltd., Oxford, 1991, pp. 162-73.
23. H. Fredriksson and I. Svensson: *Metall. Trans. B*, 1976, vol. 7B, pp. 599-606.
24. H. Shahani and H. Fredriksson: *Scan. J. Metall.*, 1985, vol. 14, pp. 316-20.
25. K.J. Brondyke and P.D. Hess: *Trans. TMS-AIME*, 1964, vol. 230, pp. 1542-46.
26. G. Laslaz and P. Laty: *Am. Foundrymen's Soc. Trans.*, 1991, vol. 99, pp. 83-90.
27. S.B. Johnson and C.R. Loper: *Am. Foundrymen's Soc. Trans.*, 1969, vol. 77, pp. 360-67.
28. G.K. Sigworth: *Am. Foundrymen's Soc. Trans.*, 1983, vol. 91, pp. 7-16.
29. H.S. Carslaw and J. C. Jaeger: *Conduction of Heat in Solids*, 2nd ed., Oxford University Press, London, 1971, p. 101.
30. J. Campbell: *Brit. Foundryman*, 1969, vol. 62, pp. 147-58.